Projected shell model study of neutron-rich deformed isotopes of Sr and Zr

Sonia Verma, Parvaiz Ahmad Dar, and Rani Devi
Department of Physics and Electronics, University of Jammu, Jammu-180006, India
(Received 20 August 2007; published 25 February 2008)

The projected shell model (PSM) study of $^{98-102}$Sr and $^{100-104}$Zr nuclei is carried out. The reliability of the ground-state wave function is checked by reproducing yrast spectra and electromagnetic properties. The mechanism for the onset of sudden and large deformation at $N = 60$ is worked out. The present piece of research work has unified the two different, or conflicting, early explanations for the onset of deformation at $N = 60$ by the spherical shell model and mean-field theory.

DOI: 10.1103/PhysRevC.77.024308 PACS number(s): 21.60.Cs, 21.10.Ky, 21.10.Re, 27.60.+j

I. INTRODUCTION

Cheifetz *et al.* [1] discovered in 1970 a new region of deformation around mass number $A \sim 100$. Well-developed rotational spectra were observed in several neutron-rich isotopes of Sr and Zr during the study of the fission fragments of ^{252}Cf. The observed $B(E2; 0^+ \rightarrow 2^+)$ values were as enhanced as in the rare-earth and the actinide regions. A striking feature of the observed spectra is the sudden onset of large deformation as the neutron number changes from 58 to 60 in the Sr and Zr isotopes. The onset of deformation is large, sudden, and asymptotic. The yrast spectra in the nuclei $^{98-102}$Sr and $^{100-104}$Zr are almost rotational. The onset of large deformation is also reflected in the experimental $B(E2; 0^+ \rightarrow 2^+)$ values.

The first calculations explaining the onset of large deformation in neutron-rich nuclei in the mass region $A \sim 100$ were done by Federman and Pittel [2–6]. They have tried to identify some of the factors that could be held responsible for the observed onset of large deformation at neutron number 60 in Zr and Mo isotopes. These calculations, which involved considerably restricted valence space, provided some evidence suggesting that the neutron-proton (n-p) interaction between the valence particles in the spin-orbit partner (SOP) orbits—the orbits $1g_{9/2}$ and $1g_{7/2}$ in the present context—may be responsible for the observed large deformation in Zr isotopes. The role of the n-p interaction in the SOP orbits in the context of the general development of the collective features was also suggested by the shell-model configuration mixing calculations for the nucleus ^{98}Zr carried out by Federman *et al.* [4]. These calculations involved the Yukawa force with Rosenfeld admixture in conjunction with the valence configuration $(2p_{1/2}, 1g_{9/2}, 2d_{5/2})_{2\pi}$ and $(3s_{1/2}, 2d_{3/2}, 1g_{7/2}, 1h_{11/2})_{2\upsilon}$ outside the ^{94}Sr core. It was observed that the degree of collectivity of the wave functions for the first excited 0^+ level, as reflected in the extent of configuration mixing, depended very much on the relative energy separation between $(1g_{9/2})_\pi$ and $(1g_{7/2})_\upsilon$ orbits.

There is another school of thought put forth by mean-field theorists [7–9] who have assigned the development of large deformations in Zr isotopes to the occupation of low K components of the $h_{11/2}$ neutron orbit. Their mean-field calculations indicate the appearance of $K = 1/2, 3/2$ components of $h_{11/2}$ neutron orbits at the Fermi surface in ^{100,102}Zr isotopes. They claim that since this orbit is down-sloping, its occupation brings in prolate deformation in the nucleus and becomes a triggering mechanism for the development of collectivity in $^{100-104}$Zr. It was shown in Refs. [10–12] that a phenomenological quadrupole-quadrupole plus pairing model of two-body interactions is quite reliable in this mass region.

Thus, a paradoxical situation exists in the mass region $A = 100$. One does not really understand whether the onset of sudden and asymptotic deformation at neutron number $N = 60$ should be attributed to the role of the deformation-producing tendency of n-p interaction in SOP orbits or to the occupation of the down-sloping $K = 1/2, 3/2$ components of the $h_{11/2}$ orbit by the neutrons as this orbit appearing at the the Fermi surface as neutron number becomes 60. To have a deeper understanding of the problem, it is important to look at the limitation of the earlier calculations. Limitations could be in the choice of the core, valence space, and two-body residual interaction, which could produce an inaccurate wave function. Thus, it is important to check the reliability of the determinantal wave function that is suggestive of these two mechanisms for the onset of large deformation at $N = 60$.

From quantum mechanics, we know that information about all observable quantities for a quantum system is just contained in the wave function of the system. If the wave function is truely representative of $^{100-104}$Zr, then it should reproduce not only the deformation trend in $^{100-104}$Zr but also other observable quantities as well. It is very much possible for two different state functions to reproduce the deformation effects say in ^{100}Zr, without being truly the representative of ^{100}Zr. The true test of the wave function is to see whether it reproduces all other observable quantities such as high-spin yrast spectra, angular-momentum-dependent moment of inertia, $B(E2)$ transition probabilities and nuclear "g" factors. Unfortunately, many of the earlier calculations [2–7,9,13–19], have not made this attempt and hence the reliability of their state function cannot be ascertained. There are some calculations wherein $B(E2)$ values, excitation spectra, and g factors have been calculated [10–12,20,21]. From the results presented in calculations [10–12,21], the agreement for $B(E2)$ values has been obtained by varying the effective charges for protons and neutrons from isotope to isotope. In the case of excitation energy spectra, except for the 2_1^+ state, the agreement for higher states is far from satisfactory. This, therefore, creates doubt as to whether

the wave function generated in these calculations is truly representative of ^{100}Zr.

Further, the advent of sophisticated experimental tools has made it possible to obtain experimentally the high-spin states, $B(E2)$ transition probabilities, and nuclear g factors [20,22–29]. The ground-state bands of $^{100-104}$Zr are presently established up to $20^+, 20^+$, and 14^+, respectively [23]. Recently, eight new high-spin states have been identified from studies of ^{252}Cf spontaneous fission with Gammasphere [24] in ^{100}Zr. Levels in ^{102}Zr were first studied by Cheifetz *et al.* [1]. Recently, Hua *et al.* [23] have extended the yrast band up to 20^+. The quadrupole deformation parameter (β_2) ~ 0.39 has been derived from life time measurement by Jared *et al.* [30]. Therefore, a region of large deformation is observed in heavy even-even nuclei at ^{102}Zr. The level scheme of ^{104}Zr has been extended up to 14^+ by Hua *et al.* [23]. Experimentally, ^{104}Zr with $\beta_2 = 0.47(7)$ has a larger deformation than that of ^{102}Zr. The nucleus ^{98}Sr is well deformed. The ground-state band of ^{98}Sr, in particular, exhibits excellent rotational properties with a large and rigid moment of inertia. ^{98}Sr is predicted to have a well-deformed prolate ground state. ^{100}Sr is the most deformed neutron-rich isotope. The levels in ^{100}Sr were observed at the CERN-ISOLDE facility in a β-decay study of ^{100}Rb by Azuma *et al.* [31]. Further members of the ground-state band up to $I^\pi = 10^+$ were identified in prompt-fission studies [32].

It is known from the literature that the projected shell model (PSM) has become quite popular for studying the structure of deformed nuclei [33–38]. The advantage of this method is that the numerical requirement is minimal and therefore it is possible to perform a systematic study for a group of nuclei in a reasonable time frame. The PSM approach is based on the diagonalization in the angular-momentum-projected basis from the deformed Nilsson states. This approach produced good agreement in the rare-earth region [39,40]. Looking at the success of PSM framework in the rare-earth region, we were tempted to use this approach for the deformed Sr and Zr isotopes.

In the present study an attempt has been made to study the deformed $^{98-102}$Sr and $^{100-104}$Zr isotopes in the framework of PSM by employing a quadrupole-quadrupole plus monopole and quadrupole pairing force in the Hamiltonian.

The main emphasis of the present paper is first to establish the reliability of the determinantal wave function by making a calculation of the other important observable quantities such as high-spin yrast states, $B(E2)$ transition probabilities, and nuclear g factors, all of which are very sensitive to the accuracy and reliability of the wave function. Unfortunately, this could not be done earlier as the data on high-spin states and nuclear g factors have only recently become available [20,22–25].

II. PROJECTED SHELL MODEL

For a detailed description of PSM theory, the reader is referred to the review article [41]. Here, we present an outline of the model. For the present study, we include 0-, 2-, and 4-quasiparticle (qp) states $|\Phi_\kappa\rangle$ as

$$\left\{|0\rangle, \alpha^+_{\upsilon_i}\alpha^+_{\upsilon_j}, |0\rangle, \alpha^+_{\pi_m}\alpha^+_{\pi_n}|0\rangle, \alpha^+_{\upsilon_i}\alpha^+_{\upsilon_j}\alpha^+_{\pi_m}\alpha^+_{\pi_n}|0\rangle\right\}, \tag{1}$$

for doubly even nuclei, where a^+ is the creation operator for a single quasiparticle and the index $\upsilon(\pi)$ denotes neutrons (protons). The many-body wave function is a superposition of projected (angular momentum) multiquasiparticle states,

$$|\psi^I_M\rangle = \sum_{\kappa K} f^I_{\kappa K} P^I_{MK}|\phi_\kappa\rangle, \tag{2}$$

where P^I_{MK} are the angular-momentum-projection operators. The coefficients $f^I_{\kappa K}$ are the weights of the basis state κ and are determined by the diagonalization of the shell-model Hamiltonian in the space spanned by the projected basis states given. Because of the presence of axial symmetry and omission of particle number projection, the set of quantum numbers κ contains the total intrinsic magnetic quantum number K implicitly. We can therefore omit writing K in the amplitude $f^I_{\kappa K}$ for such a system. Moreover, the summations over K can also be omitted since only one specific K contributes to the sum for a given κ. This leads to the set of equations on which the present numerical calculations are based:

$$\sum_{\kappa'}\left(H^I_{\kappa\kappa'} - EN^I_{\kappa\kappa'}\right) f^I_{\kappa'} = 0,$$

where the Hamiltonian and norm matrix elements are defined by

$$H^I_{\kappa\kappa'} = \langle\phi_\kappa|\hat{H}\hat{P}^I_{KK'}|\phi_{\kappa'}\rangle$$

and

$$N^I_{\kappa\kappa'} = \langle\phi_\kappa|\hat{P}^I_{KK'}|\phi_{\kappa'}\rangle.$$

The projection of an intrinsic state, $|\phi_\kappa\rangle$, onto a good angular momentum will generate the rotational energy as

$$E_\kappa(I) = \frac{\langle\phi_\kappa|\hat{H}\hat{P}^I_{KK}|\phi_\kappa\rangle}{\langle\phi_\kappa|\hat{P}^I_{KK}|\phi_\kappa\rangle} = \frac{H^I_{\kappa\kappa}}{N^I_{\kappa\kappa}}.$$

It represents the expectation value of the Hamiltonian with respect to a projected quasiparticle state κ. A diagram in which rotational energies of various bands are plotted against the spin I will be referred to as a band diagram. Such diagrams contain incredibly rich information.

The usual separable-force Hamiltonian [41]

$$H = \hat{H}_0 - \frac{\chi}{2}\sum_\mu \hat{Q}^+_\mu\hat{Q}_\mu - G_M\hat{P}^+\hat{P} - G_Q\sum_\mu \hat{P}^+_\mu\hat{P}_\mu \tag{3}$$

has been used successfully to explain the system of rotational spectra for a large number of nuclei. The first term is the spherical single-particle Hamiltonian

$$\hat{H}_0 = \sum_\alpha c^+_\alpha E_\alpha c_\alpha, \tag{4}$$

where c^+_α, c_α are the single-particle creation and annihilation operators, respectively, and E_α is the single-particle energy given by

$$E_\alpha = \hbar\omega[N - 2\kappa\hat{l}\cdot\hat{s} - \kappa\mu(\hat{l}^2 - \langle\hat{l}\rangle^2)], \tag{5}$$

where ω is the harmonic-oscillator parameter, which incorporates the principle of volume conservation for nuclei deformed from spherical shapes, and s and l represent the intrinsic nucleon spins and orbital momenta in the stretched coordinate

basis. The Nilsson parameters κ and μ are taken from the N-dependent values of Refs. [42,43]. The remaining terms in Eq. (3) are residual quadrupole-quadrupole, monopole pairing, and quadrupole pairing interactions, respectively. The strength χ of the quadrupole-quadrupole term can be obtained via self-consistent conditions with a given deformation parameter, β_2, so it is not a true parameter. The value of β_2 was set by varying it around the experimental value so as to reproduce the E_2^+-E_0^+ energy gap. In our calculations we have taken three major shells $N = 2, 3$, and 4 for protons and 3, 4, and 5 for neutrons. The size of the qp basis in the present case is about 67. The operators appearing in Eq. (3) are defined as [41]

$$\hat{Q}_\mu = \sum_{\alpha\beta} c_\alpha^+ Q_{\mu\alpha\beta} c_\beta,$$

$$Q_{\mu\alpha\alpha'} = \sqrt{\frac{4\pi}{5}} \delta_{NN'} \langle Njm| \left(\frac{r}{b}\right)^2 Y_{2\mu} |N'j'm'\rangle,$$

$$\hat{P}^+ = \frac{1}{2} \sum_\alpha c_\alpha^+ c_{\bar{\alpha}}^+$$

$$\hat{P}_\mu^+ = \frac{1}{2} \sum_{\alpha\beta} c_\alpha^+ Q_{\mu\alpha\beta} c_{\bar{\beta}}^+.$$

The strength of the quadrupole-quadrupole force was adjusted such that the known (input) quadrupole deformation (β_2) is obtained as a result of the self-consistent mean-field calculation. The monopole and quadrupole pairing interactions are given by

$$G_M = \left(G_1 - G_2 \frac{N-Z}{A}\right) \frac{1}{A} \text{ (MeV)}, \quad (6)$$

$$G_Q = \gamma G_M \text{ (MeV)}, \quad (7)$$

where G_M is inversely proportional to the particle number A and contains two adjustable constants G_2 and G_1 . Adjusting the parameters β_2, G_2, and G_1 will change the energy gap for each shell and thus will affect the selection of the quasiparticle basis. Here in our calculations $G_1$is taken as 20.25 for both neutrons and protons and G_2 as 16.20(0) for neutrons (protons). The strength of the quadrupole-quadrupole pairing force, G_Q, is assumed to be proportional to G_M. One may carefully adjust the ratio of G_Q/G_M during the calculation to get the best representation of experimental observation. In the present calculation, the ratio of G_Q/G_M is fixed as 0.20 for ^{98,100}Sr and 0.18 for ^{102}Sr, and $^{100-104}$Zr. These strengths are the same as employed in the previous PSM calculation for this mass region [33,34]. After diagonalizing the Hamiltonian in the quasiparticle basis, we use the lowest energy for each spin to compare with the experimental yrast energy. The resulting wave functions are usually used to compute the $B(E2)$ transition strengths and gyromagnetic g factors [39].

III. RESULTS AND DISCUSSION

A. Discussion of band diagrams

In Fig. 1, the band diagrams for $^{98-102}$Sr and $^{100-104}$Zr are displayed. From Fig. 1(a) for ^{98}Sr, one finds that the yrast spectra up to 14^+ is coincident with the ground-state band arising from the 0-qp intrinsic state. Between $14\hbar$ and $16\hbar$, the ground-state band is crossed by the 2-qp neutron band having configuration $2\upsilon h_{11/2}[-3/2, 5/2]$, $K = 1$, indicating that the states with $I^\pi > 14\hbar$ of the yrast band arise from this intrinsic state. In ^{100}Sr [Fig. 1(b)], the states up to $14\hbar$ are coincident with the ground-state band arising from the 0-qp state, after which there is a crossing from the 2-qp proton band having configuration $2\pi g_{9/2}[-3/2, 5/2]$, $K = 1$. In ^{102}Sr [Fig. 1(c)] also, the ground-state band and the yrast band up to $16\hbar$ are coincident; thereafter, the yrast states arise from the 2-qp proton band having configuration $2\pi g_{9/2}[-3/2, 5/2]$, $K = 1$. In the case of ^{100}Zr [Fig. 1(d)], the situation is slightly different in the sense that yrast states up to $12\hbar$ come from the ground-state band and thereafter the states from 14^+ to 18^+ arise from four 2-qp neutron bands having configurations $2\upsilon h_{11/2}[-3/2, 5/2]$, $K = 1, 2\upsilon h_{11/2}[1/2, -3/2]$, $K = -1, 2\upsilon h_{11/2}[-3/2, -3/2]$, $K = 0$, and $2\upsilon h_{11/2}[1/2, 5/2]$, $K = -2$ and the states after $20\hbar$ arise from the 4-qp band having configuration $2\pi g_{9/2}[-3/2, 5/2] + 2\upsilon h_{11/2}[1/2, -3/2]$, $K = 0$. In ^{102}Zr [Fig. 1(e)], the states of the yrast band up to 12^+ are coincident with the ground-state band. Thereafter there are three bands that cross the ground-state band having configurations $2\pi g_{9/2}[-3/2, 5/2]$, $K = 1, 2\upsilon h_{11/2}[-3/2, 5/2]$, $K = 1$, and $2\upsilon h_{11/2}[5/2, 5/2]$, $K = 0$, which produce the higher angular momentum states of the yrast band. In ^{104}Zr [Fig. 1(f)], the yrast band up to 18^+ is coincident with the ground-state band. The states with $I^\pi > 18\hbar$ arise from the bands having configuration $2\pi g_{9/2}[-3/2, 5/2]$, $K = 1$, $2\upsilon h_{11/2}[-3/2, 5/2]$, $K = 1$, $2\upsilon h_{11/2}[1/2, 1/2]$, $K = 0$, $2\upsilon h_{11/2}[5/2, -7/2]$, $K = -1, 2\upsilon h_{11/2}[5/2, 5/2]$, $K = 0$, and $2\pi g_{9/2}[-3/2, 5/2] + 2\upsilon h_{11/2}[-3/2, -5/2]$, $K = 2$.

From the study of the theoretical band diagrams, it is clear that the deformation systematics and the asymptotic onset of deformation in the deformed $^{98-102}$Sr and $^{100-104}$Zr isotopes depend entirely on the nature of the ground-state band, which in turn depends on the 0-qp intrinsic state. Thus, the information regarding the factors and the mechanism of the onset of large asymptotic deformation in the Sr, Zr region is mostly contained in the 0-qp intrinsic state of these isotopes.

B. Yrast spectra

In Fig. 2, the comparison of experimental and calculated yrast spectra is presented for $^{98-102}$Sr and $^{100-104}$Zr. As is evident from the graphs of Fig. 2, the agreement between the theoretical results and the experimentally available spectra is very good. In^{98}Sr, the maximum difference between the theory and the observed value of energy for the 12^+ is 0.087 MeV. For ^{100}Zr, the maximum difference between the theory and the observed value for $I = 12^+$ is 0.428 MeV. Here, the spectra is reproduced up to 20^+. In ^{102}Zr, the spectra up to 20^+ are reproduced. Here the maximum difference for the observed and the theoretical value for $I^\pi = 20\hbar$ is 0.379 MeV. The agreement of ^{104}Zr up to 14^+ is also good.

C. Discussion of moment of inertia versus square of rotational frequency

In Fig. 3, the plots of moment of inertia ($J^{(1)}$) versus the square of the rotational frequency (ω^2) for $^{98-102}$Sr and

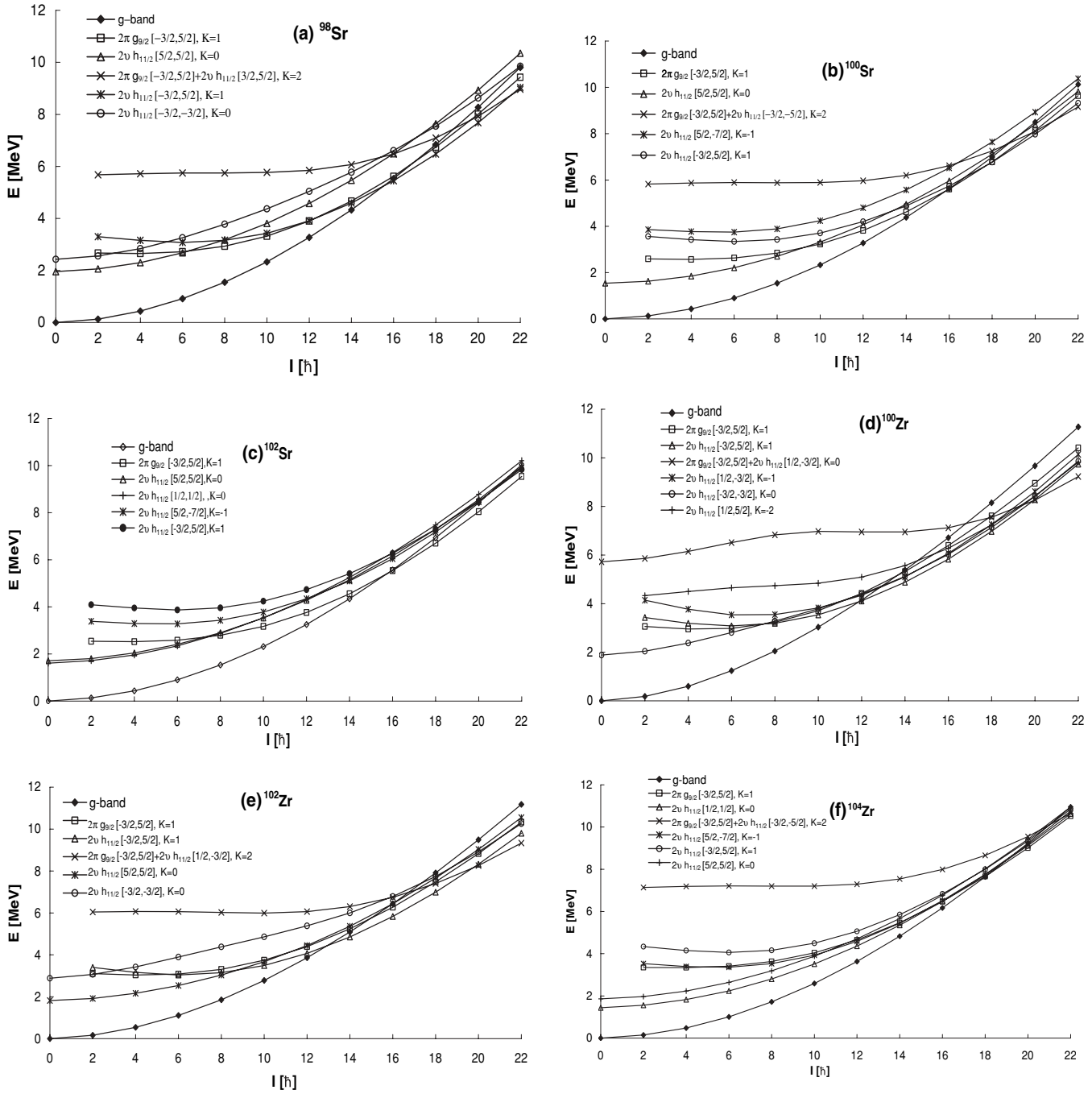

FIG. 1. Band diagrams (bands before configuration mixing) for $^{98-102}$Sr and $^{100-104}$Zr. Only the important lowest lying bands in each configuration are shown.

$^{100-104}$Zr are presented. The kinematic moment of inertia $J^{(1)}$ is defined as

$$J^{(1)} = [(I - 1/2)/\omega](\hbar^2\,\mathrm{MeV}^{-1})$$

and rotational frequency (ω) is defined as

$$\omega = [E(I) - E(I-2)]/2(\hbar\,\mathrm{MeV}).$$

From Figs. 3(a), 3(b), 3(c), 3(e), and 3(f), the experimental and theoretical curves show similar trend, however, in Fig. 3(d) for ^{100}Zr , the theoretical moment of inertia shows an upbending at 10^+, that is not exhibited by the experimental values. The trend of the $J^{(1)} - \omega^2$curve up to $10\hbar$matches with the experimental curve.

D. Discussion of $B(E2; 2_1^+ \rightarrow 0_1^+)$ and $g(2_1)$ values

$B(E2)$ transition probabilities can give important information on the nuclear structure and provide a stringent test of a particular model.

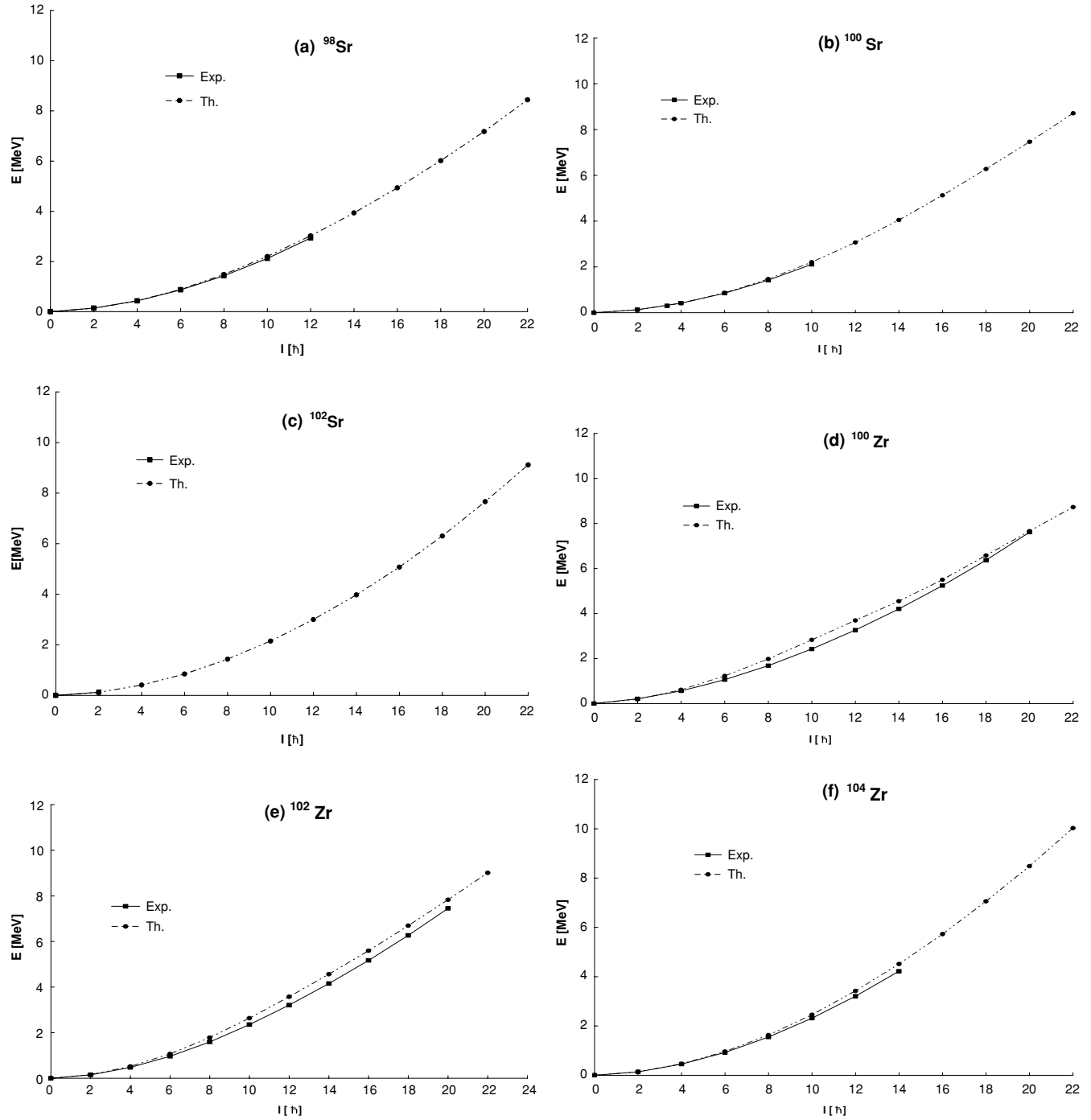

FIG. 2. Comparison of calculated yrast spectra with the experimental data for $^{98-102}$Sr and $^{100-104}$Zr.

The matrix elements of a quadrupole operator $\hat{Q}_{LM}$ with respect to the (final) shell-model wave functions can be evaluated by using the formula [41]

$$\langle \psi_{I_f M_f} | \hat{Q}_{LM} | \psi_{I_i M_i} \rangle = (I_i M_i, LM | I_f M_f) \langle \psi_{I_f} \| \hat{Q}_L \| \psi_{I_i} \rangle. \quad (8)$$

The reduced transition probabilities $B(EL)$ from the initial state I_i to the final state I_f are given by [39]

$$B(\mathrm{EL}, I_i \to I_f) = \frac{e^2}{(2I_i+1)} |\langle \psi_{I_f} \| \hat{Q}_L \| \psi_{I_i} \rangle|^2, \quad (9)$$

where the reduced matrix element is given by

$$\begin{aligned} \langle \psi_{I_f} \| \hat{Q}_L \| \psi_{I_i} \rangle &= \sum_{\kappa_i, \kappa_f} f^{I_i}_{\kappa_i} f^{I_f}_{\kappa_f} \sum_{M_i, M_f, M} (-)^{I_f - M_f} \\ &\times \begin{pmatrix} I_f & L & I_i \\ -M_f & M & M_i \end{pmatrix} \\ &\times \langle \phi_{\kappa_f} | \hat{P}^{I_f}_{K_{\kappa_f} M_f} \hat{Q}_{LM} \hat{P}^{I_i}_{K_{\kappa_i} M_i} | \phi_{\kappa_i} \rangle \\ &= 2 \sum_{\kappa_i, \kappa_f} f^{I_i}_{\kappa_i} f^{I_f}_{\kappa_f} \sum_{M', M''} (-)^{I_f - K_{\kappa_f}} (2I_f + 1)^{-1} \end{aligned}$$

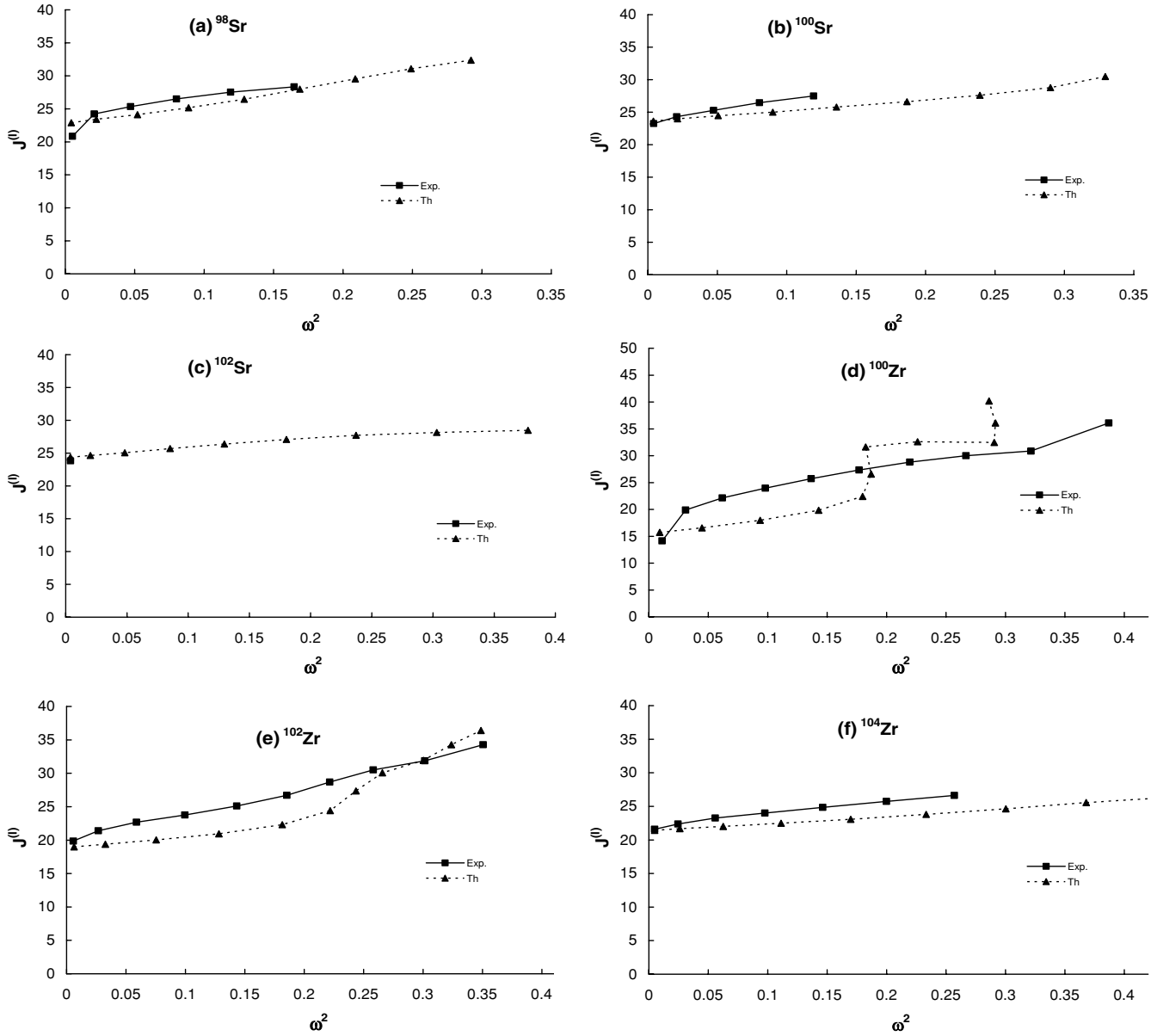

FIG. 3. Comparison of calculated moment of inertia ($J^{(1)}$) with experimental one as a function of square of rotational frequency (ω^2) for $^{98-102}$Sr and $^{100-104}$Zr.

$$\times \begin{pmatrix} I_f & L & I_i \\ -K_{\kappa_f} & M' & M'' \end{pmatrix} \int \mathbf{d}\Omega D_{M''K_{\kappa_i}}(\Omega) \times \left\langle \phi_{\kappa_f} \middle| \hat{Q}_{LM'} \hat{R}(\Omega) \middle| \phi_{\kappa_i} \right\rangle \tag{10}$$

The g factors $g(I)$, $g_\pi(I)$, and $g_\nu(I)$ are defined by [39]

$$g(I) = \frac{\mu(I)}{\mu_N I} = g_\pi(I) + g_\nu(I), \tag{11}$$

with

$$g_\tau(I) = \frac{1}{\mu_N [I(I+1)]^{1/2}} \times \left[g_l^\tau \langle \psi_I \| \hat{J}^\tau \| \psi_I \rangle + \left(g_s^\tau - g_l^\tau \right) \langle \psi_I \| \hat{S}^\tau \| \psi_I \rangle \right] \tag{12}$$

and $\mu(I)$ is the magnetic moment of a state (I).

In our calculations, the standard values of g_l and g_s have been taken as $g_l^\pi = 1$, $g_l^\upsilon = 0$, $g_s^\pi = 5.586 \times 0.75$, and $g_s^\upsilon = -3.826 \times 0.75$.

In Table I, the electromagnetic properties such as $B(E2)$ transition probabilities and g factors are presented. The $B(E2)$ values have been calculated by taking a single value of effective charge (i.e., 0.5) for all six deformed nuclei $^{98-102}$Sr and $^{100-104}$Zr. The agreement between the theoretical and the experimental values of $B(E2)$ and g factors wherever available is reasonably good.

From what has been said, it is clear that the agreement of the theoretical results with the experiments for the energy spectra, moment of inertia, $B(E2)$ transition probabilities, and nuclear g factors is reasonably good. This type of agreement leads one to conclude that the ground-state wave function,

TABLE I. Comparison of experimental (Exp.) and calculated (Th.) $B(E2)$ reduced transition probabilities (in units of e^2b^2) and g factors in $^{98-102}$Sr and $^{100-104}$Zr. Data from Refs. [20,22,25,26,29].

Nucleus	Transition	$B(E2; 2_1^+ \to 0_1^+)$		$g(2_1^+)$factor	
		Exp.	Th.	Exp.	Th.
^{98}Sr	$2_1^+ \to 0_1^+$	0.258(3)	0.338	+0.38(7)	0.341
^{100}Sr	$2_1^+ \to 0_1^+$	0.288(6)	0.352		0.360
^{102}Sr	$2_1^+ \to 0_1^+$		0.368		0.356
^{100}Zr	$2_1^+ \to 0_1^+$	0.22(1)	0.26	+0.30(3)	0.304
^{102}Zr	$2_1^+ \to 0_1^+$	0.32(4)	0.31	+0.22(5)	0.261
^{104}Zr	$2_1^+ \to 0_1^+$	0.40(6)	0.39		0.251

which contains information regarding the mechanism of the onset of large deformation, is very reliable. One intends to look for the factors that produce the right kind of deformation in these nuclei. From the analysis of the band diagrams, we have already found that the deformation systematics in $^{98-102}$Sr and $^{100-104}$Zr arise from the corresponding 0-qp intrinsic state, which is the true representative of the corresponding nuclei in view of the good agreement that has been obtained for the other observable quantities for these nuclei. To obtain those factors we have analyzed the intrinsic state vis-a-vis shell-model orbits that are occupied in these intrinsic states.

IV. DEFORMATION SYSTEMATICS

From the systematics of 2^+ states in $^{98-102}$Sr and $^{100-104}$Zr (see Table II), it is observed that the energy of the 2^+ state decreases from its value of 0.212 MeV in ^{100}Zr, to 0.151 MeV in ^{102}Zr, giving an indication that there is an increase in the degree of deformation as one goes from ^{100}Zr to ^{102}Zr. This fact is also confirmed by the increase in the ratio E_4^+/E_2^+. The value of this ratio for ^{100}Zr is 2.66 whereas its value for ^{102}Zr is 3.16. Besides this, it is observed that the 2^+ state suffers a very small change as one moves from ^{100}Zr to ^{104}Zr. This small change is indicative of the fact that the onset of deformation in ^{100}Zr is asymptotic and there is very little chance of increasing deformation thereafter. This is also indicated by the small change in the value of E_4^+/E_2^+. The value of this ratio for ^{102}Zr is 3.16 whereas its value for ^{104}Zr is 3.25. A similar trend is also observed in deformed Sr nuclei. For ^{98}Sr, E_2^+ is 0.144 MeV and E_4^+/E_2^+ is 3.0, whereas in ^{100}Sr, E_2^+ is 0.129 MeV and the E_4^+/E_2^+ ratio is 3.23. The last two columns of Table II display the experimental and theoretical quadrupole deformation parameters for $^{98-102}$Sr and $^{100-104}$Zr. The theoretical β_2 values listed in Table II are actually the input deformation parameters for the deformed basis and have been varied around the experimental value so as to reproduce the E_2^+–E_0^+ energy gap. The theoretical values follow the same trend as is exhibited by the experimental values. The theoretical values are in close agreement with the experimental values, thereby showing that the deformation systematics are qualitatively reproduced. The value obtained theoretically for β_2 is 0.35 for ^{98}Sr whereas the observed value is 0.40. Similarly, in the case of ^{100}Zr, the observed and the calculated values for β_2 are 0.32 and 0.30, respectively. For ^{102}Zr, the values are 0.39 and 0.32, respectively. We note that theoretical values of β_2 show a marginal increase as one goes from one isotope to the other, indicating that the onset of deformation is asymptotic.

We next focus our attention on the factors that could be responsible for the deformation of neutron-rich Sr and Zr isotopes. In this regard, it is important to discuss and highlight some of the well-accepted factors responsible for bringing sizeable collectivity in nuclei in the same region. It is generally felt that the n-p effective interaction possesses a deformation-producing tendency and the neutron-neutron (n-n) or proton-proton (p-p) effective interactions are mostly of spherifying nature [2,6,44–47]. These ideas have played a pivotal role in the development of the stretch scheme [45] of Danos and Gillet, the rotor model [46] of Arima and Gillet, and the interacting boson model of Arima *et al.* [47]. In this regard, the role of the n-p interaction in SOP orbits in the context of the general development of collective features was also suggested by Federman and Pittel [2–5] and Casten [48]. Their calculations provided evidence suggesting that the n-p interaction between the valence nucleons in the SOP orbits- $(1g_{9/2})_\pi$ and $(1g_{7/2})_\upsilon$ in the zirconium nuclei may be instrumental vis-à-vis the observed set of deformation in Zr isotopes with $A \geqslant 100$. It may be pointed out that the role of the n-p interaction between the SOP orbits in producing deformation depends critically on the relative occupation probabilities of $(1g_{9/2})_\pi$ and $(1g_{7/2})_\upsilon$ orbits [49].

TABLE II. Comparison of experimental (Exp.) and calculated (Th.) excitation energies (in units of MeV) of $2_1^+(E_2^+)$, $4_1^+(E_4^+)$, E_4^+/E_2^+ ratio, and deformation parameter (β_2) in $^{98-102}$Sr and $^{100-104}$Zr. Data from Refs. [15,23–28,32].

Nucleus	Exp.			Th.			β_2	
	E_2^+	E_4^+	E_4^+/E_2^+	E_2^+	E_4^+	E_4^+/E_2^+	Exp.	Th.
^{98}Sr	0.144	0.433	3.00	0.131	0.430	3.28	0.409(5)	0.350
^{100}Sr	0.129	0.417	3.23	0.127	0.419	3.29	0.426	0.350
^{102}Sr	0.126			0.123	0.408	3.31		0.350
^{100}Zr	0.212	0.564	2.66	0.191	0.614	3.21	0.32	0.300
^{102}Zr	0.151	0.478	3.16	0.158	0.519	3.28	0.39	0.320
^{104}Zr	0.139	0.452	3.25	0.140	0.463	3.30	0.47(7)	0.360

TABLE III. The BCS subshell occupation number of the various (a) proton (b) neutron subshells in ground states of the $^{96-102}$Sr and $^{98-104}$Zr.

(a) BCS subshell occupation number

Nucleus	$2p_{1/2}$	$2p_{3/2}$	$1f_{5/2}$	$1f_{7/2}$	$3s_{1/2}$	$2d_{3/2}$	$2d_{5/2}$	$1g_{7/2}$	$1g_{9/2}$
^{96}Sr	0.74	3.46	3.76	7.88	0.01	0.02	0.16	0.1	1.89
^{98}Sr	0.59	2.33	3.17	7.84	0.09	0.05	0.81	0.08	3.01
^{100}Sr	0.59	2.33	3.18	7.84	0.07	0.05	0.81	0.08	3.01
^{102}Sr	0.58	2.32	3.18	7.85	0.07	0.05	0.81	0.08	3.00
^{98}Zr	1.13	3.73	4.73	7.91	0.01	0.02	0.12	0.08	2.27
^{100}Zr	0.65	3.12	3.57	7.87	0.07	0.06	0.72	0.13	3.78
^{102}Zr	0.64	3.00	3.51	7.86	0.08	0.08	0.79	0.15	3.84
^{104}Zr	0.64	2.72	3.44	7.84	0.12	0.14	0.92	0.22	3.93

(b) BCS subshell occupation number

Nucleus	$3s_{1/2}$	$2d_{3/2}$	$2d_{5/2}$	$1g_{7/2}$	$1g_{9/2}$	$3p_{1/2}$	$3p_{3/2}$	$2f_{5/2}$	$2f_{7/2}$	$1h_{9/2}$	$1h_{11/2}$
^{96}Sr	0.36	0.60	3.20	3.09	9.74	0.005	0.01	0.01	0.10	0.04	0.88
^{98}Sr	0.58	0.96	2.24	2.95	9.06	0.02	0.17	0.05	1.02	0.06	2.91
^{100}Sr	0.59	1.00	2.68	3.28	9.43	0.03	0.18	0.06	1.12	0.09	3.52
^{102}Sr	0.60	1.03	3.15	3.78	9.62	0.03	0.20	0.09	1.20	0.11	4.14
^{98}Zr	0.28	0.45	3.56	3.05	9.77	0.006	0.01	0.02	0.08	0.05	0.80
^{100}Zr	0.54	0.92	2.44	2.99	9.41	0.014	0.11	0.03	0.8	0.052	2.741
^{102}Zr	0.57	0.97	2.82	3.38	9.55	0.02	0.14	0.04	0.99	0.06	3.42
^{104}Zr	0.61	1.05	3.09	3.75	9.57	0.05	0.22	0.11	1.24	0.14	4.14

In the mean-field approach, the deformation in the Zr isotopes has generally been explained in terms of two unrelated features, namely, the polarization of the $Z = 40$ core and the participation of the $h_{11/2}$ neutron orbit in the configuration space. The deformation in Zr is seen to arise through crossing of $1h_{11/2}; \pm 1/2, \pm 3/2$ levels at the Fermi surface.

To understand how deformation arises in Sr and Zr isotopes, we present in Table III the results of occupation probabilities of various proton and neutron subshells. These occupation probabilities have been calculated from the BCS intrinsic state. From Table III(a), it is observed that $2p_{1/2}$, $2p_{3/2}$, and $1f_{5/2}$ proton subshells are polarized and partially filled. The polarization of these subshells will be one of the important factors contributing to the appearance of deformation in Sr and Zr isotopes. Second, it is observed from this table that the the $1g_{9/2}$ proton occupation is sizeable even for nuclei ^{96}Sr and ^{98}Zr for which $N = 58$. For these very nuclei, one notices from Table III(b) that there are neutrons in the$1g_{7/2}$ subshell. Thus, there is an opportunity for n-p interaction in SOP orbits to operate (the $1g_{9/2}$ proton and $1g_{7/2}$ neutron orbits in this case). If the n-p interaction operating between the SOP orbits was a dominant effect then ^{96}Sr and ^{98}Zr should also have been deformed, which is actually not the case. It is therefore a weak deformation-producing effect. Thus, one could conclude that this factor alone cannot lead to large deformation in Sr and Zr isotopes. As pointed out by Federman and Pittel [5], this factor could also be one of the factors contributing to the onset of deformation in Sr and Zr isotopes. From Table III(b), we also notice that low K components of $1h_{11/2}$ and $2f_{7/2}$ neutron orbits are getting occupied in ^{96}Sr to ^{102}Sr and ^{98}Zr to ^{104}Zr and these occupation probabilities undergo sharp increase as one goes from ^{96}Sr to ^{98}Sr and from ^{98}Zr to ^{100}Zr. Since these low K components are sharply down-sloping, their occupation could also lead to deformation in these isotopes. The occupation of low K components of the $(1h_{11/2})_\upsilon$ orbit has been claimed to be the mechanism behind the large onset of deformation in Zr isotopes by mean-field theorists [7–9]. Moreover, one notices that the $2d_{5/2}$ and $1g_{7/2}$ neutron subshells are less than half full and could therefore also contribute to the buildup of deformation in heavy Sr and Zr isotopes.

From this discussion, it is evident that there are a number of factors responsible for bringing in deformation in neutron-rich Sr and Zr isotopes at neutron number $N = 60$. The results clearly point out that the simultaneous polarization of $2p_{1/2}$, $2p_{3/2}$, and $1f_{5/2}$ proton orbits is one of the major factors of onset of deformation. The second factor is the sharp increase in the $1g_{9/2}$ proton occupation as one goes from ^{96}Sr to ^{98}Sr and from ^{98}Zr to ^{100}Zr. The third factor responsible for the deformation systematics in neutron-rich Sr and Zr isotopes is the occupation of low K components of $1h_{11/2}$ and $2f_{7/2}$ neutron orbits. The last (but not the least) factor that could also contribute to the deformation in this region is the fact that $2d_{5/2}$ and $1g_{7/2}$ neutron subshells are less than half full.

The present calculation reveals that all these conditions hold true simultaneously in the deformed Sr and Zr isotopes. These factors are therefore acting in unison and are responsible for the sudden onset of large and asymptotic deformation in Sr and Zr isotopes.

V. CONCLUSIONS

From the results of our calculation, the following conclusions can be drawn:

(i) The PSM calculations performed with the quadrupole-quadrupole interaction plus monopole and quadrupole

pairing force reproduces correctly the observed deformation systematics in $^{98-102}$Sr and $^{100-104}$Zr isotopes. The deformation develops because of the following effects, all of which take place simultaneously in these nuclei:

(a) the simultaneous polarization of $2p_{1/2}$, $2p_{3/2}$, and $1f_{5/2}$ proton orbits,
(b) the sharp increase in the $g_{9/2}$ proton occupation as we go from ^{96}Sr to ^{98}Sr and from ^{98}Zr to ^{100}Zr,and
(c) the occupation of low K components of $1h_{11/2}$ and $2f_{7/2}$ neutron orbits, and
(d) the fact that $2d_{5/2}$ and $1g_{7/2}$ neutron subshells are less than half full.

(ii) The reasonably good agreement of the theoretical results with the experimental data for the energy states, moment of inertia , $B(E2)$ transition probabilities, and g factors test the reliability of the PSM wave function.

ACKNOWLEDGMENTS

The authors are most grateful to Prof. Y. Sun and Prof. J. A. Sheikh for their Collaboration and most valuable discussions. One of the authors (R.D.) is thankful to DST, New Delhi, for providing financial assistance under the minor SERC FAST TRACK DST Project No. SR/FTP PS-23/2004.

[1] E. Cheifetz, R. C. Jared, S. G. Thompson, and J. B. Wilhelmy, Phys. Rev. Lett. **25**, 38 (1970).
[2] P. Federman and S. Pittel, Phys. Lett. **B69**, 385 (1977).
[3] P. Federman and S. Pittel, Phys. Lett. **B77**, 29 (1978).
[4] P. Federman, S. Pittel, and R. Campos, Phys. Lett. **B82**, 9 (1979).
[5] P. Federman and S. Pittel, Phys. Rev. C **20**, 820 (1979).
[6] S. Pittel, Nucl. Phys. **A347**, 417 (1980).
[7] P. Bonche, H. Flocard, P. H. Heenen, S. J. Kreiger, and M. S. Weiss, Nucl. Phys. **A443**, 39 (1985).
[8] X. Campi and M. Epherre, Phys. Rev. C **22**, 2605 (1980).
[9] T. R. Werner, J. Dobaczewski, M. W. Guidry, W. Nazarewicz, and J. A. Sheikh, Nucl. Phys. **A578**, 1 (1994).
[10] S. K. Sharma, P. N. Tripathi, and S. K. Khosa, Phys. Rev. C **38**, 2935 (1988).
[11] P. N. Tripathi, S. K. Sharma, and S. K. Khosa, Phys. Rev. C **29**, 1951 (1984).
[12] S. K. Khosa, P. N. Tripathi, and S. K. Sharma, Phys. Lett. **B119**, 257 (1982).
[13] A. Faessler, J. E. Galonska, U. Gotz, and H. C. Pauli, Nucl. Phys. **A230**, 302 (1974).
[14] E. Kirchuk, P. Federman, and S. Pittel, Phys. Rev. C **47**, 567 (1993).
[15] A. Baran and W. Hohenberger, Phys. Rev. C **52**, 2242 (1995).
[16] J. Skalski, P. H. Heenen, and P. Bonche, Nucl. Phys. **A559**, 221 (1993).
[17] M. Sugita and A. Arima, Nucl. Phys. **A515**, 77 (1990).
[18] G. A. Lalazissis and M. M. Sharma, Nucl. Phys. **A586**, 201 (1995).
[19] M. Bhattacharya and G. Gangopadhyay, Phys. Rev. C **75**, 017301 (2007).
[20] A. G. Smith, D. Patel, G. S. Simpson, R. M. Wall, J. F. Smith, O. J. Onkanmi, I. Ahmad, J. P. Greene, M. P. Carpenter, T. Lauritsen, C. J. Lister, R. V. F. Janssens, F. G. Kondev, D. Seweryniak, B. J. P. Gall, O. Dorvaux, and B. Roux, Phys. Lett. **B591**, 55 (2004).
[21] A. Chandan, T. A. War, N. Sawhney, A. Bharti, and S. K. Khosa, Ind. J. Phys. **78**, 965 (2004).
[22] S. Raman, C. W. Nestor Jr., and P. Tikkanen, At. Data Nucl. Data Tables **78**, 1 (2001).
[23] H. Hua, C. Y. Wu, D. Cline, A. B. Hayes, R. Teng, R. M. Clark, P. Fallon, A. Goergen, A. O. Macchiavelli, and K. Vetter, Phys. Rev. C **69**, 014317 (2004).
[24] J. K. Hwang, A. V. Ramayya, J. H. Hamilton, J. O. Rasmussen, Y. X. Luo, D. Fong, K. Li, C. Goodin, S. J. Zhu, S. C. Wu, M. A. Stoyer, R. Donangelo, X.-R. Zhu, and H. Sagawa, Phys. Rev. C **74**, 017303 (2006).
[25] J. K. Hwang, A. V. Ramayya, J. H. Hamilton, Y. X. Luo, A. V. Daniel, G. M. Ter-Akopian, J. D. Cole, and S. J. Zhu, Phys. Rev. C **73**, 044316 (2006).
[26] H. Mach, F. K. Wohn, G. Molnar, K. Sistemich, J. C. Hill, M. Moszynski, R. L. Gill, W. Krips, and D. S. Brenner, Nucl. Phys. **A523**, 197 (1991).
[27] M. A. C. Hotchkis, J. L. Durell, J. B. Fitzgerald, A. S. Mowbray, W. R. Phillips, I. Ahmad, M. P. Carpenter, R. V. F. Janssens, T. L. Khoo, E. F. Moore, L. R. Morss, Ph. Benet, and D. Ye, Nucl. Phys. **A530**, 111 (1991).
[28] D. De Frenne and E. Jacobs, Nucl. Data Sheets **83**, 535 (1998).
[29] A. Wolf, K. Sistemich, H. Mach, R. L. Gill, R. F. Casten, and J. A. Winger, Phys. Rev. C **40**, 932 (1989).
[30] R. C. Jared, H. Nifenecker, and S. G. Thompson, in *Proceedings of the Third Symposium on Physics and Chemistry of Fission, IAEA Rochester, New York* (IAEA-SM-174, Vienna, 1974), Vol. II, p. 211.
[31] R. E. Azuma, G. L. Borchert, L. C. Carraz, P. G. Hansen, B. Jonson, S. Mattsson, O. B. Nielsen, G. Nyman, I. Ragnarsson, and H. L. Ravn, Phys. Lett. **B86**, 5 (1979).
[32] J. H. Hamilton, A. V. Ramayya, S. J. Zhu, G. M. Ter-Akopian, Yu. Oganessian, J. D. Cole, J. O. Rasmussen, and M. A. Stoyer, Prog. Part. Nucl. Phys. **35**, 635 (1995).
[33] J. Doring, G. D. Johns, M. A. Riley, S. L. Tabor, Y. Sun, and J. A. Sheikh, Phys. Rev. C **57**, 2912 (1998).
[34] R. Palit, J. A. Sheikh, Y. Sun, and H. C. Jain, Nucl. Phys. **A686**, 141 (2001).
[35] R. Palit, H. C. Jain, P. K. Joshi, J. A. Sheikh, and Y. Sun, Phys. Rev. C **63**, 024313 (2001).
[36] R. Palit, H. C. Jain, P. K. Joshi, and J. A. Sheikh, Pramana J. Phys. **57**, 191 (2001).
[37] S. Verma, R. Devi, and S. K. Khosa, Eur. Phys. J. A **30**, 531 (2006).
[38] P. A. Dar, R. Devi, S. K. Khosa, and J. A. Sheikh, Phys. Rev. C **75**, 054315 (2007).
[39] Y. Sun and J. L. Egido, Nucl. Phys. **A580**, 1 (1994).
[40] K. Hara and Y. Sun, Nucl. Phys. **A529**, 445 (1991).
[41] K. Hara and Y. Sun, Int. J. Mod. Phys. E **4**, 637 (1995).
[42] T. Bengtsson and I. Ragnarsson, Nucl. Phys. **A436**, 14 (1985).

[43] R. A. Meyer, E. Monnand, J. A. Pinston, F. Schussler, I. Ragnarsson, B. Pfeiffer, H. Lawin, G. Lhersonneau, T. Seo, and K. Sistemich, Nucl. Phys. **A439**, 510 (1985).
[44] S. C. K. Nair, A. Ansari, and L. Satpathy, Phys. Lett. **B71**, 257 (1977).
[45] M. Danos and V. Gillet, Phys. Rev. C **161**, 1034 (1967).
[46] A. Arima and V. Gillet, Ann. Phys. (NY) **66**, 117 (1971).
[47] A. Arima, T. Otsuka, F. Iachello, and I. Talmi, Phys. Lett. **B66**, 205 (1977).
[48] R. F. Casten, Nucl. Phys. **A443**, 1 (1985).
[49] P. K. Mattu and S. K. Khosa, Phys. Rev. C **39**, 2018 (1989).